HHS Public Access

Author manuscript

Magn Reson Med. Author manuscript; available in PMC 2020 May 01.

Published in final edited form as:

Magn Reson Med. 2019 May ; 81(5): 3065–3079. doi:10.1002/mrm.27632.

Mapping water exchange across the blood-brain barrier using three-dimensional diffusion-prepared arterial spin labeled perfusion MRI

Xingfeng Shao[1], **Samantha J Ma**[1], **Marlene Casey**[1], **Lina D'Orazio**[2], **John M Ringman**[2], and **Danny JJ Wang**[1,2,*]

[1]Laboratory of FMRI Technology (LOFT), Mark & Mary Stevens Neuroimaging and Informatics Institute, Keck School of Medicine, University of Southern California

[2]Department of Neurology, Keck School of Medicine, University of Southern California

Abstract

Purpose: To present a novel MR pulse sequence and modeling algorithm to quantify the water exchange rate (k_w) across the BBB without contrast, and to evaluate its clinical utility in a cohort of elderly subjects at risk of cerebral small vessel disease (SVD).

Methods: A diffusion preparation module with spoiling of non-CPMG signals was integrated with pseudo-continuous ASL (pCASL) and 3D GRASE readout. The tissue/capillary fraction of the ASL signal was separated by appropriate diffusion weighting (b=50s/mm^2). k_w was quantified using a single-pass approximation (SPA) model with total generalized variation (TGV) regularization. Nineteen elderly subjects were recruited and underwent two MRIs to evaluate the reproducibility of the proposed technique. Correlation analysis was performed between k_w and vascular risk factors, clinical dementia rating (CDR) scale, neurocognitive assessments and white matter hyper-intensity (WMH).

Results: The capillary/tissue fraction of ASL signal can be reliably differentiated with the diffusion weighting of b=50 s/mm^2, given ~100-fold difference between the (pseudo) diffusion coefficients of the two compartments. Good reproducibility of k_w measurements (ICC=0.75) was achieved. Average k_w was 105.0±20.6, 109.6±18.9 and 94.1±19.6 min^{-1} for whole brain, gray and white matter. k_w was increased by 28.2%/19.5% in subjects with diabetes/hypercholesterolemia. Significant correlations between k_w and vascular risk factors, CDR, executive/memory function and the Fazekas scale of WMH were observed.

Conclusion: A diffusion prepared 3D GRASE pCASL sequence with TGV regularized SPA modeling was proposed to measure BBB water permeability non-invasively with good reproducibility. k_w may serve as an imaging marker of cerebral SVD and associated cognitive impairment.

*Corresponding Author: Danny JJ Wang, PhD, MSCE, Laboratory of FMRI Technology (LOFT), Mark & Mary Stevens Neuroimaging and Informatics Institute, Keck School of Medicine, University of Southern California (USC), jwang71@gmail.com, Phone: 323-442-7246.

Keywords

Blood-brain barrier (BBB); Arterial spin labeling (ASL); Water permeability; Diffusion; Perfusion; Gradient and spin echo (GRASE); Small vessel disease (SVD)

INTRODUCTION

The blood-brain barrier (BBB) is formed in part by the endothelial cells of cerebral blood vessels with intercellular tight junctions (TJs) (1,2). The BBB plays a critical role in regulating the delivery of oxygen and nutrients to the brain, clearance of toxic metabolites, and protection of the central nervous system (CNS) from infection (3). Accumulating experimental and clinical evidence indicate that compromised or impaired BBB is associated with a number of serious CNS diseases including multiple sclerosis (MS), stroke, brain tumors, CNS infection, small vessel disease (SVD) and Alzheimer's disease (AD) (1,3–5).

Recent evidence suggests that the BBB has limited permeability to water molecules as well (6–13). Within the CNS, the TJs between BBB endothelium cells and the lack of fenestrations in the endothelium itself prohibit water filtration. The majority of water molecules pass through the BBB via "water channels" consisting of a protein termed aquaporin (14). With a diameter on the order of a single water molecule, aquaporin only allows for diffusion of one molecule at a time (15). This limited water exchange across the BBB has physiological significance in protecting the brain from edema and swelling. This effect therefore provides the physiological basis for using water exchange rate as a surrogate index of BBB integrity and permeability.

Existing imaging approaches to assess BBB permeability include PET and MRI by monitoring the (dynamic) uptake of contrast agents in brain tissue. PET, a method that is expensive and involves radioactivity, has been the primary tool used by the pharmaceutical industry to assess the CNS uptake of radioisotope labeled ligands or candidate drugs with high specificity (16). To date, dynamic contrast-enhanced (DCE) MRI using intravenous injection of gadolinium (Gd) based contrast agents (GBCAs) has been the most widely applied method for imaging BBB permeability in clinical settings (17). Quantitative analysis of the degree of BBB permeability (expressed as the volume transfer constant, K_{trans}) has been achieved using pharmacokinetic modeling (18,19), or alternatively using first-pass T2*-weighted dynamic susceptibility contrast (DSC) MRI (20,21). However, GBCAs can have complications in persons with compromised kidney function, and have been linked to permanent Gadolinium deposition in the brain, especially in persons undergoing repeated scans. Both the US FDA and ISMRM have recently issued statements to limit the use of GBCAs to clinical circumstances in which the additional information provided by the contrast is necessary (22).

An alternative to exogenous contrast agents is water, which is an abundant and endogenous tracer with limited permeability across BBB. Since GBCAs have relatively large molecular weights (Gd-DTPA 550 Da), BBB permeability has to reach a critical level before extravasation occurs (23,24). Water molecules have much smaller molecular weight, assessing BBB water permeability could potentially provide a more direct and sensitive

biomarker of BBB function at the early stage of disease progression. Arterial spin labeling (ASL) perfusion MRI permits noninvasive measurement of cerebral blood flow using magnetically labeled water as an endogenous tracer. Water exchange across the BBB can be quantified based on ASL signal fractions in the intra- and extravascular compartments. Diffusion-weighted (DW) ASL techniques have been proposed to differentiate the fraction of labeled water in capillary and brain tissue based on their distinctive (pseudo) diffusion coefficients (high in capillary and low in tissue) (13,25). This DW ASL technique has recently been validated by mannitol administration to open BBB and using an ischemia-reperfusion model to disrupt BBB in rats (26,27). Altered BBB water permeability has been detected by DW ASL in subjects with obstructive sleep apnea compared to controls (28).

However, existing DW ASL techniques employed 2D echo-planar imaging (EPI) readout resulting in relatively low SNR and reliability. The purpose of this study was to present a new pulse sequence with diffusion prepared pseudo-continuous ASL (pCASL) with background suppressed 3D gradient and spin echo (GRASE) readout. The test-retest reproducibility of this diffusion prepared 3D GRASE pCASL sequence was evaluated with repeated scans approximately 2 weeks apart. The clinical utility for detecting subtle changes of BBB permeability was evaluated by performing the proposed sequence in a cohort of elderly subjects at risk of cerebral SVD through correlations of water permeability with known risk factors and behavioral phenotypes of SVD.

THEORY

Modeling of water exchange rate (kw) across BBB

According to the Renkin-Crone equation (29,30), the permeability surface product of water (PS_w) can be calculated based on the water extraction ratio (E_w) and cerebral blood flow (CBF):

$$PS_w = -\ln(1 - E_w) \times CBF \quad [1]$$

To estimated E_w, a long post-labeling delay (PLD) is usually required to allow complete extraction of labeled water into tissue space (31). Due to T1 relaxation, the low SNR of remaining ASL signal makes it impractical to generate reliable voxel-wise water exchange rate map.

St Lawrence, et al, proposed a single-pass approximation (SPA) solution to model pCASL signal in the capillary and brain tissue compartments while incorporating the exchange rate of water from blood to tissue (k_w) (12):

$$\Delta M_c(t) = -\frac{2\varepsilon \cdot CBF \cdot M_0}{\lambda(k_w + R_{1a})} e^{-(R_{1a} - (k_w + R_{1a}))ATT} \left(e^{-(k_w + R_{1a})(t-\delta)} - e^{-(k_w + R_{1a})t}\right) \quad [2]$$

$$\Delta M_b(t) = -\frac{2\varepsilon \cdot CBF \cdot M_0}{\lambda(k_w + R_{1a})} \cdot \frac{k_w}{k_w + (R_{1a} - R_{1b})}\left[\frac{e^{-(R_{1a} - R_{1b})ATT}}{R_{1b}}\left(e^{-R_{1b}(t-\delta)} - e^{-R_{1b}t}\right)\right. \quad [3]$$
$$\left. - \frac{e^{-(R_{1a} - (k_w + R_{1a}))ATT}}{(k_w + R_{1a})}\left(e^{-(k_w + R_{1a})(t-\delta)} - e^{-(k_w + R_{1a})t}\right)\right]$$

where $\Delta M_c(t)$ and $\Delta M_b(t)$ are ASL signals from the capillary and tissue space, respectively; ε is labeling efficiency, δ is labeling duration, λ is the partition coefficient of water in the brain, R_{1a} and R_{1b} are the longitudinal relaxation rate of arterial blood and brain tissue, respectively. R_{1a} was assumed to be 0.601 s^{-1} (32). Voxel-wise R_{1b} map was fitted from background suppressed control images acquired at two PLDs according to (33). The water exchange rate k_w, defined as capillary permeability surface-area product of water (PS_w) divided by distribution volume of water tracer in the capillary space (V_c), was calculated based on a monotonic relationship with the fraction of capillary signal at a given arterial transit time (ATT), as demonstrated by figure 2 in (25):

$$\begin{aligned} k_w &= f(A_1, ATT) \\ A_1 &= \frac{\Delta M_c(t)}{\Delta M_c(t) + \Delta M_b(t)} \end{aligned} \quad [4]$$

where f was derived from Eqs. [2, 3]. Capillary signal would be suppressed by a small diffusion gradient due to its pseudo random motion, and A_1 can be calculated by:

$$A_1 = 1 - \frac{\Delta M_{b_{DW}}}{\Delta M_0} \quad [5]$$

where $\Delta M_{b-value}^{PLD}$ is ASL signal with specific post-labeling delay (PLD) (ms) and b-value (s/mm^2) indicated by superscript and subscript respectively. The appropriate diffusion gradient with a weighting of b_{DW}, which suppresses capillary signal while imparting minimal effect on tissue signal, can be determined by bi-exponential fitting of the DW pCASL signals acquired at multiple b-values. ATT was estimated by the flow-encoding arterial spin tagging (FEAST) method (34), as a function of the ratio of the vascular suppressed (with diffusion weighting b_{ATT} = 14 s/mm^2, VENC = 7.5 mm/s) ASL signal to the total signal acquired at a short PLD (900 ms):

$$ATT = g\left(\frac{\Delta M_{b_{ATT}}^{900}}{\Delta M_0^{900}}\right) \quad [6]$$

Estimation of k_w with TGV regularized SPA model

According to (25), estimated k_w is sensitive to noise when tissue fraction is close to 1. A Gaussian filter can be applied to ASL images to improve SNR, however, a pre-defined threshold of k_w was still required to exclude spuriously high values in local regions. Instead of using a Gaussian filter, we propose a novel total generalized variation (TGV) regularized SPA modeling algorithm for estimating ATT and k_w. TGV is an improved mathematical framework based on minimizing both first and second-order total variation (TV) for MRI de-noising or undersampled reconstruction, which minimizes blotchy (or oil painting like) appearance in MRI images reconstructed with traditional TV algorithm (35). ATT and k_w can be estimated from DW pCASL data acquired at the PLD of 900 and 1800ms with respective b values:

$$\underset{ATT,ATT'}{\arg\min}\left[\frac{1}{2\lambda}\cdot\left\|ATT-g\left(\frac{\Delta M^{900}_{b_{ATT}}}{\Delta M^{900}_{0}}\right)\right\|_2^2+\alpha_1\left|\nabla ATT-ATT'\right|_1+\frac{\alpha_0}{2}\left|\nabla ATT'+\nabla ATT'^{T}\right|_1\right] \quad [7]$$

$$\underset{k_w,k'_w}{\arg\min}\left[\frac{1}{2\lambda}\cdot\left\|k_w-f\left(1-\frac{\Delta M^{1800}_{b_{DW}}}{\Delta M^{1800}_{0}},ATT\right)\right\|_2^2+\alpha_1\left|\nabla k_w-k'_w\right|_1+\frac{\alpha_0}{2}\left|\nabla k'_w+\nabla k'^{T}_w\right|_1\right] \quad [8]$$

where $\lambda = 0.05$ is the weighting factor balancing data fidelity and TGV penalty function, ∇ donates discrete differentiation, $\alpha_1 = 1$ and $\alpha_0 = 2$, which were recommended by (35), balances between the first and second derivative of ATT and k_w map.

METHODS

Diffusion prepared 3D pCASL pulse sequence

Figure 1 shows the diagram of the diffusion-prepared (DP) 3D GRASE pCASL sequence, which consists of 4 modules of pCASL labeling, background suppression, diffusion preparation and GRASE readout. Diffusion preparation was implemented before the GRASE readout, as shown in figure 1 (b). Diffusion gradients were formulated in bipolar pairs along the slice direction and their timing was optimized to minimize the eddy current according to (36). Non-selective pulses were used to compensate for field inhomogeneity and two refocusing pulses consisted of MLEV composite pulses to ensure robust refocusing (37). The transverse signal was then tipped-up before readout followed by spoiler gradients along three axes to destroy residual transverse magnetization.

Since bulk motion during the diffusion encoding induces spatially varying phase shift ϕ_0, an additional de-phasing gradient was applied along phase-encoding (PE) direction after the bi-polar gradients to induce a linear phase increment along PE. The purpose of this additional de-phasing gradient was to spoil the non-CPMG signal caused by ϕ_0, as originally proposed by Alsop (38). A pair of re-phasing and rewound de-phasing gradients were added before

and after each refocusing pulse to balance the gradient moment, as demonstrated in figure 1 (c).

MRI experiments

All subjects underwent MRI scans on a Siemens 3T Prisma system (Erlangen, Germany) using a 20-channel head coil after they provided informed consent according to a protocol approved by the Institutional Review Board (IRB) of the University of Southern California. A total of twenty-eight subjects participated in this study including four healthy volunteers (3 male, age = 34±11 yrs) for pulse sequence optimization, nineteen aged subjects (7 male, age=68.8±7.6 yrs, all Latinos) enrolled from the MarkVCID study (www.markvcid.org) for clinical evaluation of the developed pulse sequences and five subjects from the same cohort (2 male, age=68±6 yrs) for comparison with 2D DW-pCASL. Imaging parameters for the diffusion-prepared GRASE pCASL sequence were: FOV = 224 mm, matrix size = 64×64, 12 slices (10% oversampling), resolution = 3.5×3.5×8 mm^3, turbo factor = 14, EPI factor = 64, bandwidth = 3125 Hz/pixel, TE = 36.5 ms, TR = 4000 ms, label/control duration=1500ms, centric ordering, timing of background suppression was optimized according to (39), duration of four diffusion gradient lobes = 3.4/5.1/5.5/3.0 ms.

To determine the optimal $b_{DW,}$ the proposed sequence was performed in four healthy subjects with three PLDs (1500, 1800 and 2100 ms) and six b-values (b = 0, 10, 25, 50, 100, 200 s/mm^2). Twenty repetitions (2 mins 40 secs) were acquired for each b value. Bi-exponential fitting of ASL signals with six diffusion weightings was conducted to calculate the diffusion coefficients for capillary (D_c) and tissue (D_b) compartments, and to determine the appropriate b_{DW} which suppress capillary signal with minimal effect on tissue signal:

$$\frac{\Delta M_b}{\Delta M_0} = A_1 \cdot e^{-b \cdot D_c} + (1 - A_1) \cdot e^{-b \cdot D_b} \quad [9]$$

We employed the two-stage approach proposed by St Lawrence et al (25) to measure ATT and k_w. Fifteen repetitions were acquired for each b-value of the FEAST scan at PLD = 900 ms with a total acquisition time of 4 mins. k_w was calculated from scans acquired at PLD = 1800 ms, when the labeled blood reaches the microvascular compartment, with b=0 and b_{DW}. Twenty repetitions were acquired for each b-value of the k_w scan, and the total acquisition time was 6 mins. An extra reference image without background suppression was acquired at the PLD of 2000 ms to generate cerebral blood flow (CBF) and R_{1b} map (33). CBF was calculated from the reference image and ΔM_0^{1800} according to (40), using blood-tissue water partition coefficient = 0.9 g/ml and labeling efficiency = 77%.

Evaluation in elder subjects at risk for small vessel disease (SVD)

MRI scans were performed in a cohort of elderly subjects enrolled in the MarkVCID study. Nineteen subjects were recruited and underwent two MRIs approximately 2 weeks apart to evaluate the reproducibility of the proposed sequence. Test-retest MRI scans were conducted on similar times of the day to minimize potential effects of circadian rhythms, and subjects were abstinent from caffeine intake 3 hours before MRI scans. For comparison, 2D DW-

pCASL scans were performed in five subjects from the same cohort. Imaging parameters of the 2D DW-pCASL were: FOV = 224 mm, matrix size=64×64, 7/8 partial Fourier factor, 12 slices, ascending ordering, slice gap = 1 mm, resolution = 3.5×3.5×8mm^3, bandwidth = 3125 Hz/pixel, TE = 48 ms, TR = 4300 ms, label/control duration=1500ms. Fifteen pairs were acquired at PLD=900ms with b = 0 and 10 (VENC=7.5 mm/s) s/mm^2 and 20 pairs were acquired at PLD=1800s with b = 0 and 50 s/mm^2 respectively.

Clinical assessments

Subjects underwent a physical exam, medical history evaluation (hypertension, diabetes, hypercholesterolemia) and blood draw before the first MRI scan. Presence or absence of hypertension, diabetes and hypercholesterolemia was defined by a prior diagnosis and/or current treatment for these conditions. Vascular risk factor (0–3) was calculated as the combination of presences of hypertension, diabetes or hypercholesterolemia. Neuropsychological assessment was performed using the Alzheimer's Disease Centers' Uniform Data Set v3 (UDS3) as well as the NIH toolbox. Volumes of white matter hyperintensity (WMH) was manually segmented by a clinical fellow from T2-weighted Fluid-Attenuated Inversion Recovery (FLAIR) images (resolution = 1×1×1 mm^3, inversion time/TE/TR=1800/388/5000 ms) using ITK-SNAP (www.itksnap.org) (41). The Fazekas scale of WMH was rated for each subject according to (42). Clinical information and descriptions of all clinical assessments are summarized in Table 1.

Data analysis

Control/label images were corrected for rigid head motion off-line using SPM12 (Wellcome Trust Centre for Neuroimaging, UCL) and subtracted to obtain perfusion images. Temporal fluctuations in the difference image series owing to residual motion and physiologic noise were minimized using an algorithm based on principal component analysis (43). k_w and ATT maps were generated with TGA regularized SPA model using average DW pCASL signals acquired at the PLD of 900 and 1800ms, as well as the R_{1b} map generated from background suppressed control images in each individual subject. The alternating direction method of multipliers (ADMM, http://web.stanford.edu/~boyd/papers/admm_distr_stats.html) algorithm was implemented in Matlab to solve Eqs. [7, 8].

Average k_w and ATT were measured for the whole brain, gray matter (GM) and white matter (WM), respectively. GM and WM masks were segmented using SPM12 based on co-registered 3D magnetization prepared rapid gradient echo (MPRAGE) images. The test-retest reproducibility of average k_w and CBF in the whole brain was quantified by intra-class correlation coefficient (ICC). The k_w maps were then normalized into the canonical MNI space, and the ICC of k_w was also computed in eight regions of interests (ROIs) related to AD: frontal lobe, temporal lobe, parietal lobe, hippocampus, parahippocampal gyrus, anterior/posterior cingulum, precuneus (44). Correlation between average k_w from both test and retest scans and clinical/behavioral assessments were evaluated using mixed effects linear regression model implemented in STATA 13.1 (College Station, Texas), incorporating age and gender as covariates and time (test/retest) as the random variable. Mixed effects linear regression was also performed to evaluate the correlation between average k_w and

CBF from test and retest scans. Two significant levels were set as P value less than 0.05 and 0.005 (2-sided).

RESULTS

Optimization of 3D Diffusion Prepared pCASL

Figure 2 shows DW pCASL perfusion images of a single slice acquired at 3 PLDs and six b-values. The DW pCASL signal intensity decays with increasing PLD or b-values. Average perfusion signal intensity from four subjects (marks) and bi-exponential fitting results (curves) are shown in figure 3 (R^2 = 0.997, 0.988 and 0.996 for the bi-exponential fitting of perfusion signals at PLD = 1500, 1800 and 2100 ms respectively). On average, 76%, 85% and 89% of labeled blood enters brain tissue space at the PLD of 1500, 1800 and 2100 ms, respectively. Estimated (pseudo) diffusion coefficients of capillary/brain tissue (D_c/D_b) were 0.08/0.0010 mm^2/s, 0.09/0.0009 mm^2/s and 0.05/0.0006 mm^2/s at the PLD of 1500 ms, 1800 ms and 2100 ms, respectively. Based on these results, b_{DW} = 50 s/mm^2 and PLD = 1800 ms were chosen for subsequent k_w measurements, where perfusion signal in capillary and brain tissue compartments were 1.1% and 95.6% of its original signal intensity, respectively. In other words, perfusion signal ΔM_{50}^{1800} contains 1.1% and 98.9% of capillary and tissue signal, respectively. The differentiation between capillary and tissue space is reliable given the large diffusion coefficient difference (~100 fold) between the two compartments. A sensitivity analysis with ±20% change in b_{DW} (50 s/mm^2) would induce only ~±1% change in remaining capillary signal according to Eq. [9].

TGV regularized SPA model

Figure 4 shows the comparison results from direct SPA modeling with a Gaussian filter (first row) and the proposed SPA modeling with TGV regularization (second row). Figure 4 (a, b) show the perfusion maps acquired at the PLD of 900 ms without and with diffusion weighting for vascular signal suppression (b = 14 s/mm^2), respectively. Figure 4 (d, e) show the perfusion maps acquired at the PLD of 1800 ms without and with diffusion weighting for suppression of the microvascular/capillary signal (b = 50 s/mm^2). A 3D Gaussian filter with a full-width at half maximum (FWHM) of 5 mm was applied to obtain the perfusion images in the first row of figure 4 (a, b, d, e). Figure 4 (c) shows estimated ATT maps. Prolonged ATT is observed in the posterior area, which is consistent with previous findings (34). Figure 4 (f) shows the k_w map estimated from direct SPA modeling (first row) and the proposed TGV regularized SPA modeling (second row). Direct SPA modeling with a Gaussian filter generates smoother k_w maps while TGV regularized SPA modeling preserved the original image resolution. The local bright regions (indicated by red arrows, k_w>200 min^{-1}) with spuriously high k_w values in direct SPA modeling were suppressed by TGV regularized SPA modeling.

Test-retest repeatability of DW pCASL

Figure 5 shows six slices of k_w maps from test-retest scans (global k_w = 95.3 and 96.5 min^{-1}) acquired by the proposed sequence of one representative subject (Female, 64 yrs). Average k_w values of the whole brain acquired at the second scan are plotted against the k_w

values acquired at the first scan, as shown in figure 6 (a). A good test-retest reproducibility (ICC = 0.75) was achieved for the proposed diffusion-prepared 3D GRASE pCASL sequence, while poor reproducibility was observed for 2D DW-pCASL results (ICC=0.21) (supplemental figure S1). Table 2 summaries the average k_w and ICC values of test and retest measurements from nineteen subjects in the eight ROIs. The ICC ranges from 0.17 in parahippocampal gyrus and 0.3 in hippocampus to 0.63 in precuneus and 0.72 in frontal lobe, with an average of 0.52.

Estimated average k_w was 105.0±20.6, 109.6±18.9 and 94.1±19.6 min^{-1} for the whole brain, GM and WM, respectively, which corresponds well with the literature (25). Average ATT was 1242.1±111.1, 1220.6±100.2 and 1288.8±113.7 ms for the whole brain, GM and WM, respectively. The measured ATT values fall into the lower end of the literature values (34), which may be caused by the single-excitation of the GRASE readout as compared to the previous 2D sequential slice acquisitions.

Average global CBF = 45.6±11.6 ml/100g/min across nineteen aged subjects from both test and retest scans. CBF values of the whole brain acquired at the second scan are plotted against the CBF values acquired at the first scan, as shown in figure 6 (b). ICC = 0.85 for CBF acquired from test and retest scans. No significant correlation was found between k_w and CBF (β =0.35, P=0.22).

Evaluation of DW pCASL in Aged Subjects at Risk of SVD

Table 3 summarizes the results of mixed effects model analysis of k_w (whole brain/GM/WM) using clinical and behavioral assessments as the independent variables, age and gender as covariates and time (test-retest) as the random variable. Significant correlations with P values smaller than 0.05 and 0.005 are indicated by asterisks in the table. No significant correlations between k_w and age/gender were found in this study. Increased k_w was found in subjects with type 2 diabetes (β=25.7, P<0.001) (figure 7 (a)) and hypercholesterolemia (β=17.8, P=0.04) (figure 7 (b)), which is consistent with DCE-MRI (45) and biochemical studies (46). Increased k_w was found in subjects with higher vascular risk factors (β=9.4, P=0.02) (figure 7 (c)). Both the global (CDR-GS, β=44.6, P=0.002) and sum of box scores (CDR-SB, β=21.0, P=0.001) of the CDR were significant predictors of k_w (figure 7 (e, f)), which indicates increased BBB permeability is associated with a greater severity of functional impairment. NIH toolbox measurements: DCCs (β=−1.10, P=0.02), PSMTa (β=−0.98, P=0.03) and PSMTb (β=−1.19, P=0.001) were significant correlated with k_w, and a trend of negative correlation was found between Flanker (β=−0.58, P=0.08) and k_w (figure 7 (g-j)), which indicates increased BBB water permeability is associated with a lower level of cognitive flexibility, worse episodic memory and a trend of decreased attention/inhibitory control. k_w was also significantly correlated with the Fazekas scale of WMH (β=10.61, P=0.04) (figure 7 (d)), which indicates k_w is associated with severity of WMH. A positive correlation between k_w and WMH volume was also observed in this study but failed to reach significance (β=1.68, P=0.20).

DISCUSSION

Diffusion-prepared 3D GRASE pCASL for non-contrast k_w measurement

We proposed a new MR pulse sequence for DW-pCASL with improved test-retest repeatability by integrating a diffusion preparation module optimized for minimizing eddy current and spoiling of non-CPMG signals with 3D background suppressed 3D GRASE pCASL to quantify the water exchange rate (k_w) across the BBB. Since water molecules are much smaller than the GBCAs and trans-capillary water exchange is mainly through aquaporin, assessing k_w could potentially provide a more direct and sensitive assessment of BBB dysfunction at an earlier stage of disease progression compared to conventional contrast enhanced MRI. The proposed technique is capable of generating whole brain ATT and k_w map within 10 mins, which is comparable to or shorter than clinical DCE-MRI protocols. Without any radiation or contrast injection, the proposed technique is suitable for repeated scans for longitudinal studies or populations not suitable for DCE MRI (e.g. children and subjects with renal dysfunction). The ICC of the test and retest scans of the propose diffusion prepared 3D GRASE pCASL sequence is 0.75 for the whole brain across repeated scans two weeks apart, which is comparable to or slightly lower than reported test-retest reproducibility of ASL CBF measurements (47). Fair to good reproducibility (ICC~0.5–0.75) of k_w in ROIs was also observed except for smaller regions such as the hippocampus and parahippocampal gyrus. These data suggest that k_w may provide a reliable biomarker of BBB function to track disease progression and treatment effects in a clinical trial on SVD and/or dementia.

Three-dimensional GRASE was recommended by the ASL white paper (40) for clinical implementations of pCASL perfusion MRI (39). However, it has been challenging to combine diffusion weightings with 3D turbo-spin echo (TSE) based sequences (48). Diffusion gradients induce extra phase due to bulk motion (e.g. head movement or respiration). Violation of the CPMG condition causes rapid signal decrease in regions where induced phase is not along MG phase direction, leading to dark bands or shades in images (48). Ensuring the refocusing pulse to be exactly 180° is the most straightforward approach to avoid the phase sensitivity, which is not commonly used due to SAR limitations and a small deviation from 180° is sufficient to introduce artifacts. Motion compensated diffusion preparation has been proposed to reduce the sensitivity of TSE to bulk motion (37). However, it is not suitable for the FEAST scheme to measure ATT since vascular signal is compensated. Other methods including echo splitting (49), which doubled the echo spacing, or quadratic phase modulation of refocusing phases (50), which requires long echo train, have been proposed. However, these methods are not suitable for this study because long GRASE readout causes image blurring due to T2 relaxation. The non-CPMG diffusion preparation adopted in this study has been proven to be robust to motion, however, at the cost of half signal loss (38). In the present study, we used a relatively thick slice (8 mm) to compensate for SNR loss.

TGV Regularized SPA Modeling of BBB Water Permeability

Another innovation of the present study is TGV regularized SPA modeling. In the original SPA modeling strategy (25), the estimated k_w is very sensitive to noise when the tissue

fraction is close to 1 (see Figure. 2 of (25)). This challenge is accentuated by the relatively low SNR of ASL signals. Including spatial regularization in the SPA modeling would improve the reliability of k_w estimation, which typically employs the TV metric. The TGV is an improved mathematical framework based on minimizing both first and second-order TV to avoid blotchy appearances commonly seen in TV constrained image reconstruction (35), which has also been applied for ASL de-noising (51). In the present study, we were able to preserve the original image resolution, minimizing spuriously high k_w values while improving SNR using TGV regularized SPA modeling. Sensitivity analysis of k_w versus weighting factor λ was performed by calculating k_w in a representative subject with λ varying from 0.01 to 0.10 at a step size of 0.01, about ±5% changes of k_w was observed as compared to the k_w calculated with $\lambda = 0.05$. Using the ADMM algorithm, the average calculation time was within one minute on a stand-alone computer (2.3 GHz dual-core processor).

BBB Impairment, Cerebral Small Vessel Disease and Dementia

There is growing evidence indicating that BBB permeability increases with age and these changes are accelerated in microvascular disease and dementia (4,23,52). Loss of BBB integrity may contribute to the progression of SVD by allowing neurotoxins access to the brain and causing ionic imbalance, an inflammatory response around vessels and eventually demyelination of white matter fibers (5). Elevated levels of albumin, which does not cross intact BBB, in cerebrospinal fluid (CSF) has been reported in patients with vascular dementia (53,54). The BBB dysfunction has also been implicated in the pathogenesis of AD (55,56). Currently, assessment of BBB permeability relies on CSF sampling and/or DCE MRI using GBCAs. Biochemical assays of CSF require lumbar puncture while DCE MRI requires administration of contrast and long scan time (>15min). In addition, since albumin (66 kDa) and contrast agents (550 Da) have relatively large molecular weights, BBB permeability has to reach a critical level before extravasation occurs.

In this study, we found significantly increased k_w in subjects with type 2 diabetes and hypercholesterolemia, both of which have emerged as risk factors for SVD and AD. Hypercholesterolemia has been known to be associated with vascular pathology and dysfunction including vascular inflammation and atherosclerosis, which may lead to early breakdown of the BBB (46). Diabetes mellitus leads to glycosylation of endothelial proteins and also causes the basement membrane in the vessel wall to grow abnormally thicker and weaker. As a result, the micro-vessels in the brain and body of diabetic subjects are susceptible to micro-bleeds, protein leakage, and hypo-perfusion (57). Population based studies have shown that both diabetes and hypercholesterolemia lead to increased risk of neurodegeneration, cognitive impairment and dementia (58,59). Our observation of increased k_w in subjects with diabetes and hypercholesterolemia and total vascular risk factors is consistent with existing literature, suggesting that k_w may provide a surrogate imaging biomarker of cerebral effects of common vascular risk factors and early SVD and/or AD (45).

We also observed increased k_w in subjects with decreased neurocognitive performance including increased CDR-SB/CDR-GS scores and decreased Flanker/DCCS/PSMT. Both

CDR-SB and CDR-GS have been widely used in staging dementia severity. The Flanker, DCCS and PSMT are tests of attention/inhibitory control, cognitive flexibility and episodic memory, respectively. Increased k_w was also associated with increased Fazekas scale and showed a trend of positive correlation with WMH volume. A pathological report has associated WMH with demyelination and axonal loss (60) and clinical studies have shown associations between WMH and progressive cognitive impairment and increased risk of dementia (61). Although previous studies reported globally reduced CBF in cerebral SVD patients with greater WMHs (62), the k_w changes in nineteen subjects with potential SVD was not significantly associated with CBF changes in this study. Subjects recruited in this study are in the early stages of WMH development (average WMH volume is 2.6 cm^3), and its association with k_w will provide important opportunities to prevent brain damage due to SVD at the earliest stages and ameliorate cognitive impairment.

Alternative Noncontrast Measurement of BBB Permeability

Recently, global water extraction fraction (Ew) and PSw were determined by measuring arterially labeled blood spins that are drained into cerebral veins (31), which generates reliable results in several minutes but cannot reveal BBB permeability change in local regions. Kinetic models were proposed to map the whole brain trans-capillary water exchange based on the T2 and T2* differences in the two compartments (63,64). However, reliable and accurate quantification remains challenging due to the small differences of T2/T2*. A new method for estimating water permeability (PSw) was proposed recently by utilizing the intrinsic diffusion weighting of GRASE readout but requires sophisticated deconvolution algorithms (65). In this study, the b-value of a pair of crusher gradients in GRASE readout was 0.04, 0.09 and 0.02 s/mm^2 along x, y and z directions, respectively. The blurring effects along partition direction caused by the intrinsic diffusion weighting of GRASE readout was negligible with the full width of half maximum (FWHM) of the point spread function (PSF) smaller than 1.03/1.003 voxel size for the capillary/tissue signal. The strength of our technique is that there are two orders of magnitude difference between the (pseudo) diffusion coefficients of the intra- and extravascular spaces which can be separated by a small diffusion gradient. Although a slight variation of the diffusion coefficient (D_c/D_b) was observed at three PLDs, which is consistent with a previous study (66), the differentiation between capillary and tissue space is reliable given the large diffusion coefficient difference (~100 fold). Our sensitivity analysis showed that a ±20% change in b_{DW} only induces ~±1% change in remaining capillary signal according to Eq. [9].

There are limitations of this study. Since segmented acquisition introduces inter-segment phase inconsistency and shading artifacts, single-shot acquisition is required for the proposed diffusion prepared 3D pCASL sequence. Resolution of kw/ATT map is relatively low as compared to standard ASL studies (also to compensate for half signal loss). To improve spatial resolution, fast imaging, such as 2D CAIPI (33), and reconstruction algorithm with spatial and temporal constraints will be employed (51). For comparison of 2D and 3D k_w measurements, the sample size of 2D experiment was small. Presence of arterial and venous compartments, which were considered as non-exchangeable compartments, may bias the capillary/tissue fraction estimation. The PLD of 1800 ms was chosen to exclude/minimize the arterial and venous compartments since ATT was estimated

to be 1200–1300 ms in this study and Lin, et al, (31) reported detectable venous signal at PLD > 2500 ms. Recent studies also reported water exchange in periarterial and perivenous spaces through aquaporin (67,68). This study has demonstrated the potential of k_w as a sensitive marker of BBB permeability. However, V_c may alter in diseases (e.g. decreased V_c in diabetes due to thicken vessel wall and increased perivascular space) and complicates the understanding of the relation between k_w and PS_w. With the proposed sequence, total extraction ratio E_w and PS_w can be computed with diffusion prepared 3D pCASL signals acquired at longer PLD (>2.5s) (31), which remains to be explored in future studies.

CONCLUSIONS

A diffusion prepared 3D GRASE pCASL sequence with TGV regularized SPA modeling was proposed to measure BBB water permeability non-invasively with good reproducibility in a cohort of aged subjects at risk of SVD. This study demonstrated the capability of k_w being a surrogate imaging biomarker for SVD and early dementia. Its clinical use for the detection of BBB dysfunction before the leakage of large-molecule contrast agents awaits further evaluation.

Supplementary Material

Refer to Web version on PubMed Central for supplementary material.

ACKNOWLEDGEMENT

This work was supported by National Institute of Health (NIH) grant UH2-NS100614 and R01-EB014922. The authors are grateful to Yelong Shen and John Hartzheim for evaluation of WMH, Dr. Xuejuan Jiang for help with statistical analysis, Dr. Keith St Lawrence for help with SPA modeling, and Xucheng Zhu for help with implementing ADMM algorithm.

REFERENCE:

1. Weiss N, Miller F, Cazaubon S, Couraud PO. The blood-brain barrier in brain homeostasis and neurological diseases. Biochim Biophys Acta 2009;1788(4):842–857. [PubMed: 19061857]
2. Abbott NJ, Patabendige AA, Dolman DE, Yusof SR, Begley DJ. Structure and function of the blood-brain barrier. Neurobiol Dis 2010;37(1):13–25. [PubMed: 19664713]
3. Daneman R, Prat A. The Blood–Brain Barrier. Cold Spring Harb Perspect Biol. Volume 7; 2015 p a020412. [PubMed: 25561720]
4. Farrall AJ, Wardlaw JM. Blood-brain barrier: ageing and microvascular disease--systematic review and meta-analysis. Neurobiol Aging 2009;30(3):337–352. [PubMed: 17869382]
5. Rosenberg GA, Wallin A, Wardlaw JM, Markus HS, Montaner J, Wolfson L, Iadecola C, Zlokovic BV, Joutel A, Dichgans M, Duering M, Schmidt R, Korczyn AD, Grinberg LT, Chui HC, Hachinski V. Consensus statement for diagnosis of subcortical small vessel disease. J Cereb Blood Flow Metab 2015.
6. Paulson OB. Blood-brain barrier, brain metabolism and cerebral blood flow. Eur Neuropsychopharmacol 2002;12(6):495–501. [PubMed: 12468012]
7. Ewing JR, Cao Y, Fenstermacher J. Single-coil arterial spin-tagging for estimating cerebral blood flow as viewed from the capillary: relative contributions of intra- and extravascular signal. Magn Reson Med 2001;46:465–475. [PubMed: 11550237]
8. Li KL, Zhu X, Hylton N, Jahng GH, Weiner MW, Schuff N. Four-phase single-capillary stepwise model for kinetics in arterial spin labeling MRI. Magn Reson Med 2005;53(3):511–518. [PubMed: 15723393]

9. Parkes LM, Tofts PS. Improved accuracy of human cerebral blood perfusion measurements using arterial spin labeling: accounting for capillary water permeability. Magn Reson Med 2002;48(1):27–41. [PubMed: 12111929]
10. Silva AC, Williams DS, Koretsky AP. Evidence for the exchange of arterial spin-labeled water with tissue water in rat brain from diffusion-sensitized measurements of perfusion. Magn Reson Med 1997;38(2):232–237. [PubMed: 9256102]
11. Zhou J, Wilson DA, Ulatowski JA, Traystman RJ, van Zijl PC. Two-compartment exchange model for perfusion quantification using arterial spin tagging. J Cereb Blood Flow Metab 2001;21(4):440–455. [PubMed: 11323530]
12. St Lawrence KS, Frank JA, McLaughlin AC. Effect of restricted water exchange on cerebral blood flow values calculated with arterial spin tagging: a theoretical investigation. Magn Reson Med 2000;44(3):440–449. [PubMed: 10975897]
13. Wang J, Fernandez-Seara MA, Wang S, St Lawrence KS. When perfusion meets diffusion: in vivo measurement of water permeability in human brain. J Cereb Blood Flow Metab 2007;27(4):839–849. [PubMed: 16969383]
14. Knepper MA, Nielsen S. Peter Agre, 2003 Nobel Prize winner in chemistry. J Am Soc Nephrol 2004;15(4):1093–1095. [PubMed: 15034115]
15. Agre P The aquaporin water channels. Proc Am Thorac Soc 2006;3(1):5–13. [PubMed: 16493146]
16. Nicolazzo JA, Charman SA, Charman WN. Methods to assess drug permeability across the blood-brain barrier. J Pharm Pharmacol 2006;58(3):281–293. [PubMed: 16536894]
17. Rebeles F, Fink J, Anzai Y, Maravilla KR. Blood-brain barrier imaging and therapeutic potentials. Top Magn Reson Imaging 2006;17(2):107–116. [PubMed: 17198226]
18. Tofts PS, Kermode AG. Measurement of the blood-brain barrier permeability and leakage space using dynamic MR imaging. 1. Fundamental concepts. Magn Reson Med 1991;17(2):357–367. [PubMed: 2062210]
19. Heye AK, Culling RD, Valdes Hernandez Mdel C, Thrippleton MJ, Wardlaw JM. Assessment of blood-brain barrier disruption using dynamic contrast-enhanced MRI. A systematic review. Neuroimage Clin 2014;6:262–274. [PubMed: 25379439]
20. Johnson G, Wetzel SG, Cha S, Babb J, Tofts PS. Measuring blood volume and vascular transfer constant from dynamic, T(2)*-weighted contrast-enhanced MRI. Magn Reson Med 2004;51(5):961–968. [PubMed: 15122678]
21. Leigh R, Jen SS, Varma DD, Hillis AE, Barker PB. Arrival time correction for dynamic susceptibility contrast MR permeability imaging in stroke patients. PLoS One 2012;7(12):e52656. [PubMed: 23285132]
22. Gulani V, Calamante F, Shellock FG, Kanal E, Reeder SB, International Society for Magnetic Resonance in M. Gadolinium deposition in the brain: summary of evidence and recommendations. Lancet Neurol 2017;16(7):564–570. [PubMed: 28653648]
23. Montagne A, Barnes SR, Sweeney MD, Halliday MR, Sagare AP, Zhao Z, Toga AW, Jacobs RE, Liu CY, Amezcua L, Harrington MG, Chui HC, Law M, Zlokovic BV. Blood-brain barrier breakdown in the aging human hippocampus. Neuron 2015;85(2):296–302. [PubMed: 25611508]
24. Barnes SR, Ng TS, Montagne A, Law M, Zlokovic BV, Jacobs RE. Optimal acquisition and modeling parameters for accurate assessment of low Ktrans blood-brain barrier permeability using dynamic contrast-enhanced MRI. Magn Reson Med 2016;75(5):1967–1977. [PubMed: 26077645]
25. St Lawrence KS, Owen D, Wang DJ. A two-stage approach for measuring vascular water exchange and arterial transit time by diffusion-weighted perfusion MRI. Magn Reson Med 2012;67(5):1275–1284. [PubMed: 21858870]
26. Tiwari YV, Shen Q, Jiang Z, Li W, Long J, Fang C, Duong TQ. Measuring blood-brain-barrier permeability using Diffusion-Weighted Arterial Spin Labeling (DW-ASL): Corroboration with Ktrans and Evan's blue measurements. Proc Intl Soc Magn Reson Med 2015;23.
27. Tiwari YV, Lu J, Shen Q, Cerqueira B, Duong TQ. Magnetic resonance imaging of blood-brain barrier permeability in ischemic stroke using diffusion-weighted arterial spin labeling in rats. J Cereb Blood Flow Metab 2017;37(8):2706–2715. [PubMed: 27742887]

28. Palomares JA, Tummala S, Wang DJ, Park B, Woo MA, Kang DW, St Lawrence KS, Harper RM, Kumar R. Assessment of Water Exchange Across the Blood-Brain Barrier in Patients with Obstructive Sleep Apnea. J Neuroimaging 2015;25(6):900–905. [PubMed: 26333175]
29. Renkin EM. Transport of potassium-42 from blood to tissue in isolated mammalian skeletal muscles. Am J Physiol 1959;197:1205–1210. [PubMed: 14437359]
30. Crone C The Permeability of Capillaries in Various Organs as Determined by Use of the 'Indicator Diffusion' Method. Acta Physiol Scand 1963;58:292–305. [PubMed: 14078649]
31. Lin Z, Li Y, Su P, Mao D, Wei Z, Pillai JJ, Moghekar A, van Osch M, Ge Y, Lu H. Non-contrast MR imaging of blood-brain barrier permeability to water. Magn Reson Med 2018.
32. Lu H, Clingman C, Golay X, van Zijl PC. Determining the longitudinal relaxation time (T1) of blood at 3.0 Tesla. Magn Reson Med 2004;52(3):679–682. [PubMed: 15334591]
33. Shao X, Wang DJJ. Single shot high resolution 3D arterial spin labeling using 2D CAIPI and ESPIRiT reconstruction. 2017; Honolulu, HI, USA p 3629.
34. Wang J, Alsop DC, Song HK, Maldjian JA, Tang K, Salvucci AE, Detre JA. Arterial transit time imaging with flow encoding arterial spin tagging (FEAST). Magn Reson Med 2003;50(3):599–607. [PubMed: 12939768]
35. Knoll F, Bredies K, Pock T, Stollberger R. Second order total generalized variation (TGV) for MRI. Magn Reson Med 2011;65(2):480–491. [PubMed: 21264937]
36. Reese TG, Heid O, Weisskoff RM, Wedeen VJ. Reduction of eddy-current-induced distortion in diffusion MRI using a twice-refocused spin echo. Magn Reson Med 2003;49(1):177–182. [PubMed: 12509835]
37. Nguyen C, Fan Z, Sharif B, He Y, Dharmakumar R, Berman DS, Li D. In vivo three-dimensional high resolution cardiac diffusion-weighted MRI: a motion compensated diffusion-prepared balanced steady-state free precession approach. Magn Reson Med 2014;72(5):1257–1267. [PubMed: 24259113]
38. Alsop DC. Phase insensitive preparation of single-shot RARE: application to diffusion imaging in humans. Magn Reson Med 1997;38(4):527–533. [PubMed: 9324317]
39. Shao X, Wang Y, Moeller S, Wang DJJ. A constrained slice-dependent background suppression scheme for simultaneous multislice pseudo-continuous arterial spin labeling. Magn Reson Med 2018;79(1):394–400. [PubMed: 28198576]
40. Alsop DC, Detre JA, Golay X, Gunther M, Hendrikse J, Hernandez-Garcia L, Lu H, MacIntosh BJ, Parkes LM, Smits M, van Osch MJ, Wang DJ, Wong EC, Zaharchuk G. Recommended implementation of arterial spin-labeled perfusion MRI for clinical applications: A consensus of the ISMRM perfusion study group and the European consortium for ASL in dementia. Magn Reson Med 2015;73(1):102–116. [PubMed: 24715426]
41. Yushkevich PA, Piven J, Hazlett HC, Smith RG, Ho S, Gee JC, Gerig G. User-guided 3D active contour segmentation of anatomical structures: significantly improved efficiency and reliability. Neuroimage 2006;31(3):1116–1128. [PubMed: 16545965]
42. Fazekas F, Chawluk JB, Alavi A, Hurtig HI, Zimmerman RA. MR signal abnormalities at 1.5 T in Alzheimer's dementia and normal aging. AJR Am J Roentgenol 1987;149(2):351–356. [PubMed: 3496763]
43. Shao X, Tisdall MD, Wang DJ, van der Kouwe AJ. Prospective motion correction for 3D GRASE pCASL with volumetric navigators. International Society for Magnetic Resonance in Medicine 2017 p 0680.
44. Yan L, Liu CY, Wong KP, Huang SC, Mack WJ, Jann K, Coppola G, Ringman JM, Wang DJJ. Regional association of pCASL-MRI with FDG-PET and PiB-PET in people at risk for autosomal dominant Alzheimer's disease. Neuroimage Clin 2018;17:751–760. [PubMed: 29527482]
45. Starr JM, Wardlaw J, Ferguson K, MacLullich A, Deary IJ, Marshall I. Increased blood-brain barrier permeability in type II diabetes demonstrated by gadolinium magnetic resonance imaging. J Neurol Neurosurg Psychiatry 2003;74(1):70–76. [PubMed: 12486269]
46. Acharya NK, Levin EC, Clifford PM, Han M, Tourtellotte R, Chamberlain D, Pollaro M, Coretti NJ, Kosciuk MC, Nagele EP, Demarshall C, Freeman T, Shi Y, Guan C, Macphee CH, Wilensky RL, Nagele RG. Diabetes and hypercholesterolemia increase blood-brain barrier permeability and

brain amyloid deposition: beneficial effects of the LpPLA2 inhibitor darapladib. J Alzheimers Dis 2013;35(1):179–198. [PubMed: 23388174]

47. Chen Y, Wang DJ, Detre JA. Test-retest reliability of arterial spin labeling with common labeling strategies. J Magn Reson Imaging 2011;33(4):940–949. [PubMed: 21448961]
48. Nunes RG, Malik SJ, Hajnal JV. Single shot fast spin echo diffusion imaging with correction for non-linear phase errors using tailored RF pulses. Magn Reson Med 2014;71(2):691–701. [PubMed: 23463486]
49. Schick F SPLICE: sub-second diffusion-sensitive MR imaging using a modified fast spin-echo acquisition mode. Magn Reson Med 1997;38(4):638–644. [PubMed: 9324331]
50. Bastin ME, Le Roux P. On the application of a non-CPMG single-shot fast spin-echo sequence to diffusion tensor MRI of the human brain. Magn Reson Med 2002;48(1):6–14. [PubMed: 12111926]
51. Spann SM, Kazimierski KS, Aigner CS, Kraiger M, Bredies K, Stollberger R. Spatio-temporal TGV denoising for ASL perfusion imaging. Neuroimage 2017;157:81–96. [PubMed: 28559192]
52. Wardlaw JM, Sandercock PA, Dennis MS, Starr J. Is breakdown of the blood-brain barrier responsible for lacunar stroke, leukoaraiosis, and dementia? Stroke 2003;34(3):806–812.
53. Tomimoto H Subcortical vascular dementia. Neurosci Res 2011;71(3):193–199. [PubMed: 21821070]
54. Wallin A, Blennow K, Fredman P, Gottfries CG, Karlsson I, Svennerholm L. Blood brain barrier function in vascular dementia. Acta Neurol Scand 1990;81(4):318–322. [PubMed: 2360399]
55. Zlokovic BV. Neurovascular mechanisms of Alzheimer's neurodegeneration. Trends Neurosci 2005;28(4):202–208. [PubMed: 15808355]
56. Bowman GL, Kaye JA, Moore M, Waichunas D, Carlson NE, Quinn JF. Blood-brain barrier impairment in Alzheimer disease: stability and functional significance. Neurology 2007;68(21): 1809–1814. [PubMed: 17515542]
57. Biessels GJ, Reijmer YD. Brain changes underlying cognitive dysfunction in diabetes: what can we learn from MRI? Diabetes 2014;63(7):2244–2252. [PubMed: 24931032]
58. Ahtiluoto S, Polvikoski T, Peltonen M, Solomon A, Tuomilehto J, Winblad B, Sulkava R, Kivipelto M. Diabetes, Alzheimer disease, and vascular dementia: a population-based neuropathologic study. Neurology 2010;75(13):1195–1202. [PubMed: 20739645]
59. Solomon A, Kareholt I, Ngandu T, Winblad B, Nissinen A, Tuomilehto J, Soininen H, Kivipelto M. Serum cholesterol changes after midlife and late-life cognition: twenty-one-year follow-up study. Neurology 2007;68(10):751–756. [PubMed: 17339582]
60. Fazekas F, Kleinert R, Offenbacher H, Schmidt R, Kleinert G, Payer F, Radner H, Lechner H. Pathologic correlates of incidental MRI white matter signal hyperintensities. Neurology 1993;43(9):1683–1689. [PubMed: 8414012]
61. Debette S, Markus HS. The clinical importance of white matter hyperintensities on brain magnetic resonance imaging: systematic review and meta-analysis. BMJ 2010;341:c3666. [PubMed: 20660506]
62. Shi Y, Thrippleton MJ, Makin SD, Marshall I, Geerlings MI, de Craen AJM, van Buchem MA, Wardlaw JM. Cerebral blood flow in small vessel disease: A systematic review and meta-analysis. J Cereb Blood Flow Metab 2016;36(10):1653–1667. [PubMed: 27496552]
63. Gregori J, Schuff N, Kern R, Gunther M. T2-based arterial spin labeling measurements of blood to tissue water transfer in human brain. J Magn Reson Imaging 2013;37(2):332–342. [PubMed: 23019041]
64. He X, Raichle ME, Yablonskiy DA. Transmembrane dynamics of water exchange in human brain. Magn Reson Med 2012;67(2):562–571. [PubMed: 22135102]
65. He X, Wengler KT, Duong TQ, Schweitzer M. 3D MRI Mapping of Whole-Brain Water Permeability with Intrinsic Diffusivity Encoding of Arterial Labeled Spins (IDEALS). 2018; Paris, France p 0180.
66. Zhang X, Ingo C, Teeuwisse WM, Chen Z, van Osch MJP. Comparison of perfusion signal acquired by arterial spin labeling-prepared intravoxel incoherent motion (IVIM) MRI and conventional IVIM MRI to unravel the origin of the IVIM signal. Magn Reson Med 2018;79(2): 723–729. [PubMed: 28480534]

67. Plog BA, Nedergaard M. The Glymphatic System in Central Nervous System Health and Disease: Past, Present, and Future. Annu Rev Pathol 2018;13:379–394. [PubMed: 29195051]

68. Papadopoulos MC, Verkman AS. Aquaporin water channels in the nervous system. Nat Rev Neurosci 2013;14(4):265–277. [PubMed: 23481483]

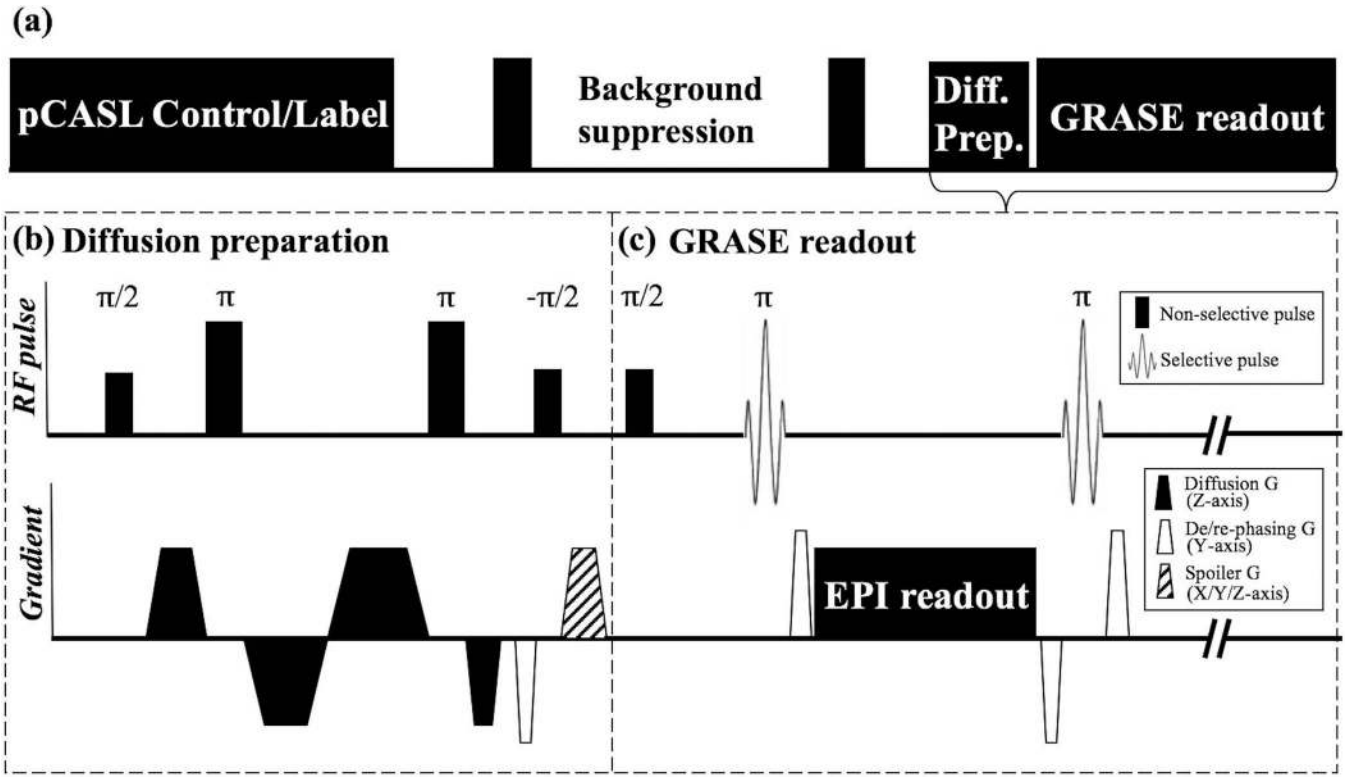

Figure 1.

(a) Sequence diagram of 3D DP-pCASL. (b) Diffusion preparation module: Non-selective pulses were used to compensate for field inhomogeneity, timing of gradients was optimized to minimize eddy current. De-phasing gradient was added along y-axis (4π dephasing per voxel) before tip-up to eliminate phase sensitivity of GRASE readout. Strong spoiler along three axes were added after tip-up to remove residual transverse magnetization. A pair of re-phasing and de-phasing gradients were added at both sides of EPI readout. (c) GRASE readout: Non-selective excitation was used to improve slab profile, re-phasing and rewound de-phasing gradients were added at two sides of EPI readout to maintain MG condition.

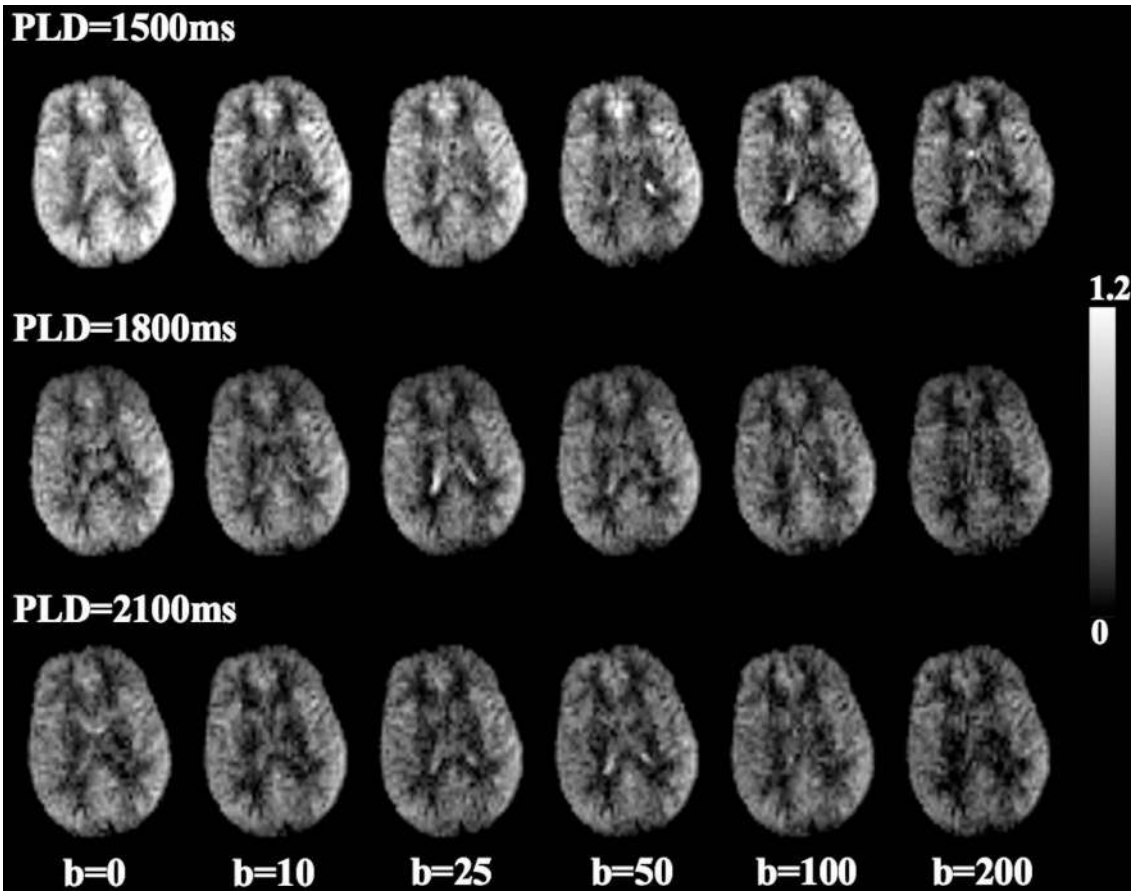

Figure 2.

Perfusion map with six diffusion weightings acquired at PLD=1500ms, 1800ms and 2100 ms, respectively. Gray scale indicates relative perfusion signal intensity compared to average perfusion signal acquired with b = 0 s/mm^2 at PLD = 1500 ms.

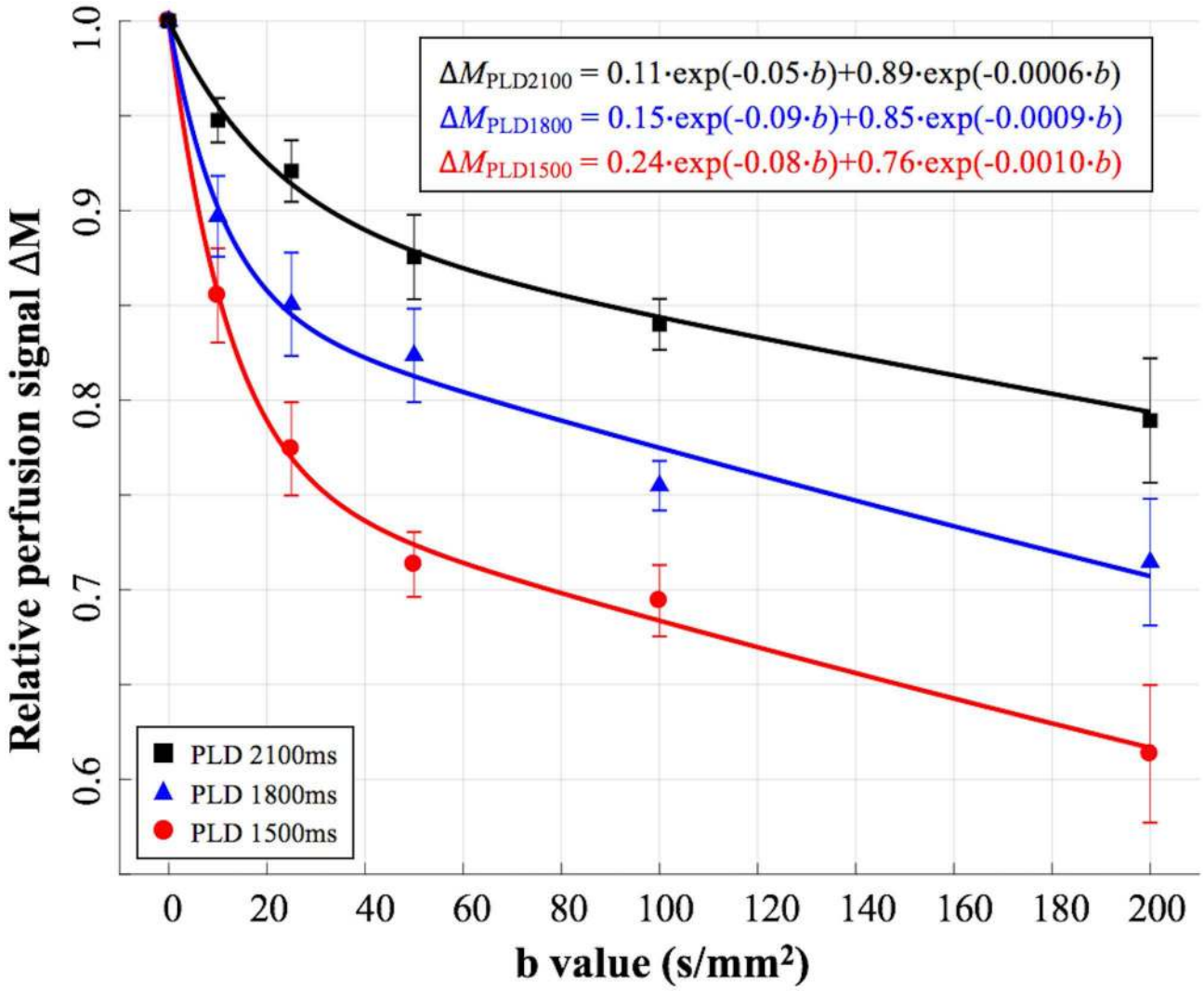

Figure 3.

Average perfusion signals from four subjects with six diffusion weightings acquired at PLD=1500ms, 1800ms and 2100ms. Error bar indicates the standard deviation of k_w measurements across four subjects. Bi-exponential fitting results are shown in the upper right corner. Capillary/tissue fraction were 24%/76% when PLD = 1500 ms, 15%/85% when PLD = 1800 ms and 11%/89% when PLD = 2100 ms, respectively.

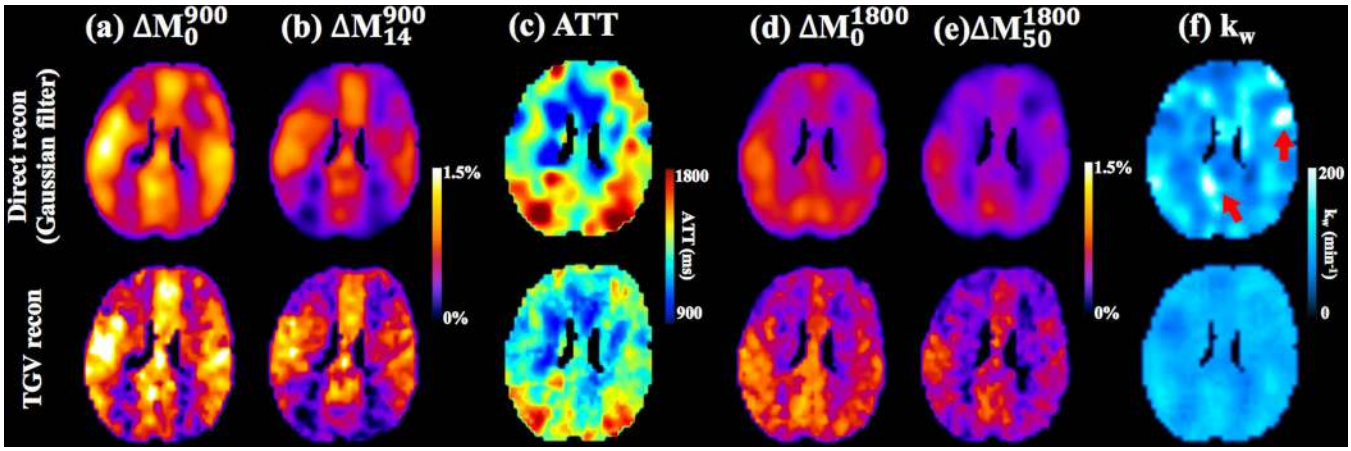

Figure 4.

Comparison of direct modeling with Gaussian smoothing (first row) and regularized SPA modeling (second row). (a) Perfusion map without diffusion weighting acquired at PLD=900ms. (b) Perfusion map with b=14 s/mm^2 (VENC=7.5cm/s to suppress vascular signal) acquired at PLD = 900 ms. (c) ATT map. (d) Perfusion map without diffusion weighting acquired at PLD = 1800 ms. (e) Perfusion map with b=50 s/mm^2 acquired at PLD = 1800ms. (f) k_w map. Red arrows indicate the local regions with noise induced spuriously high k_w values using direct modeling (first row). k_w map from regularized SPA modeling was relatively smooth (second row).

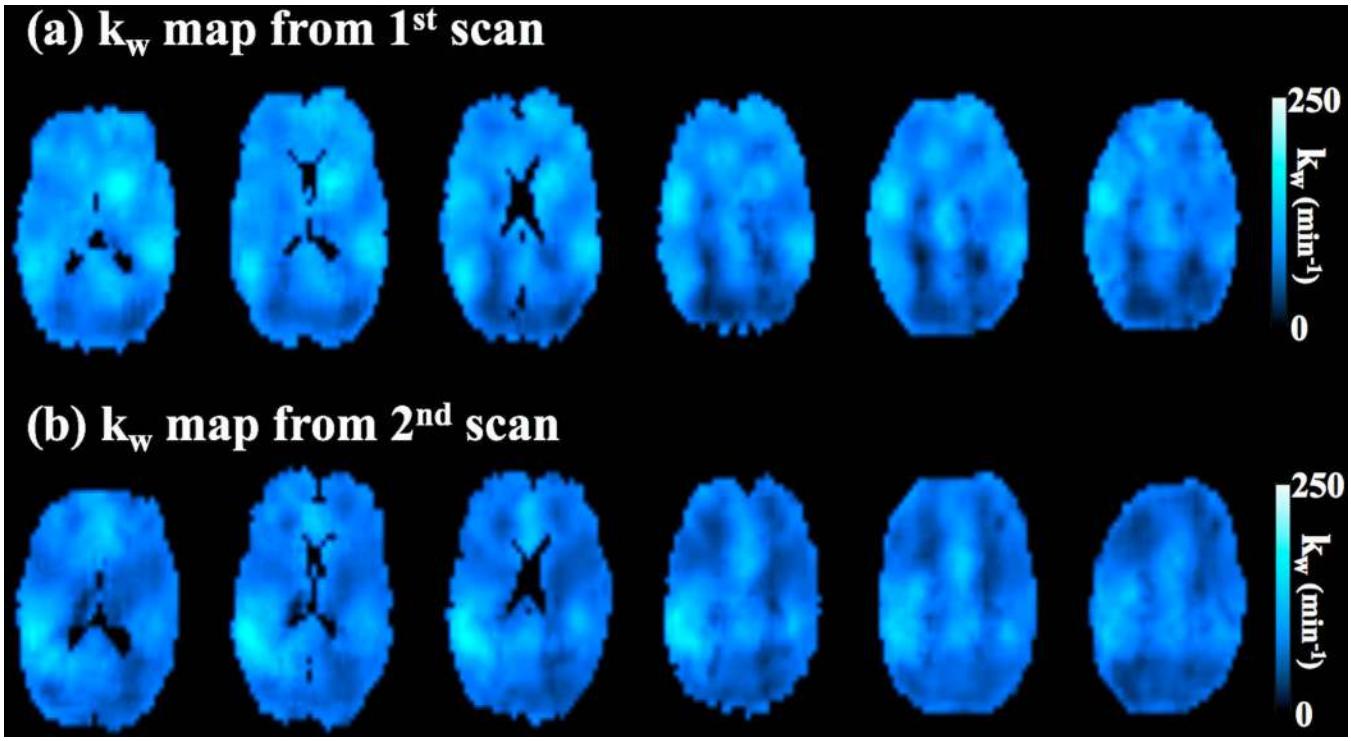

Figure 5.
k_w map of six slices from one representative subject's test and retest scans.

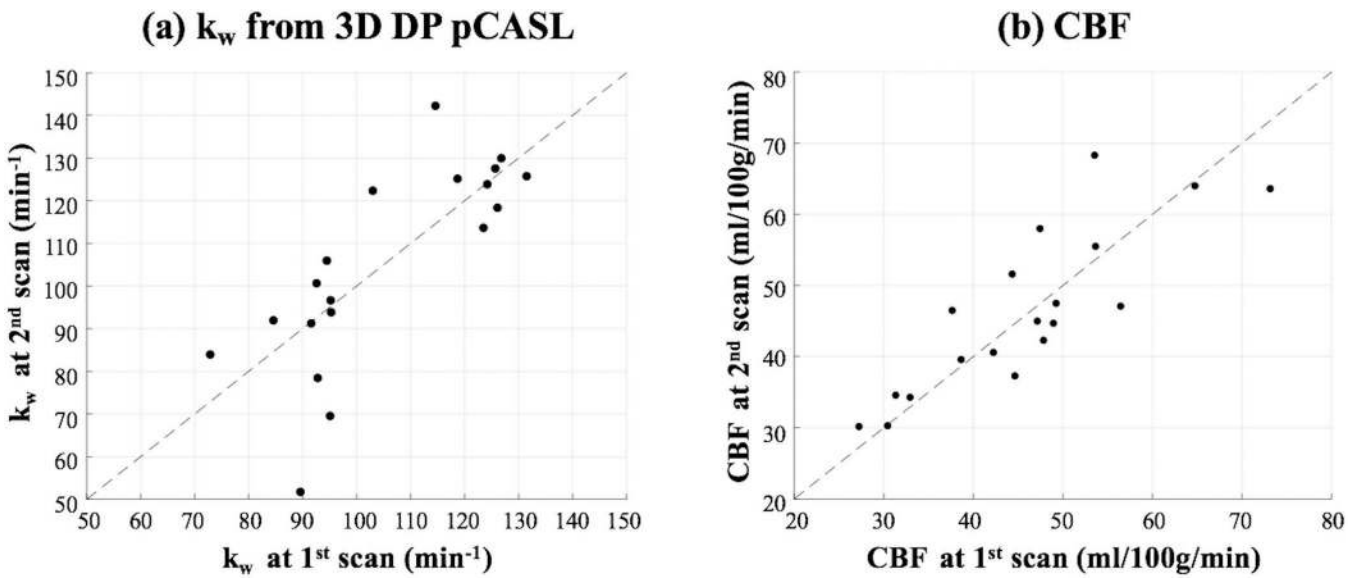

Figure 6.

(a) Average k_w values from test-retest experiments using the proposed 3D DP-pCASL sequence. Horizontal and vertical axis indicates the k_w measurements from the first and second MRI scan, respectively. (b) Average global CBF values from test-retest experiments. Horizontal and vertical axis indicates the CBF measurements from the first and second MRI scan, respectively.

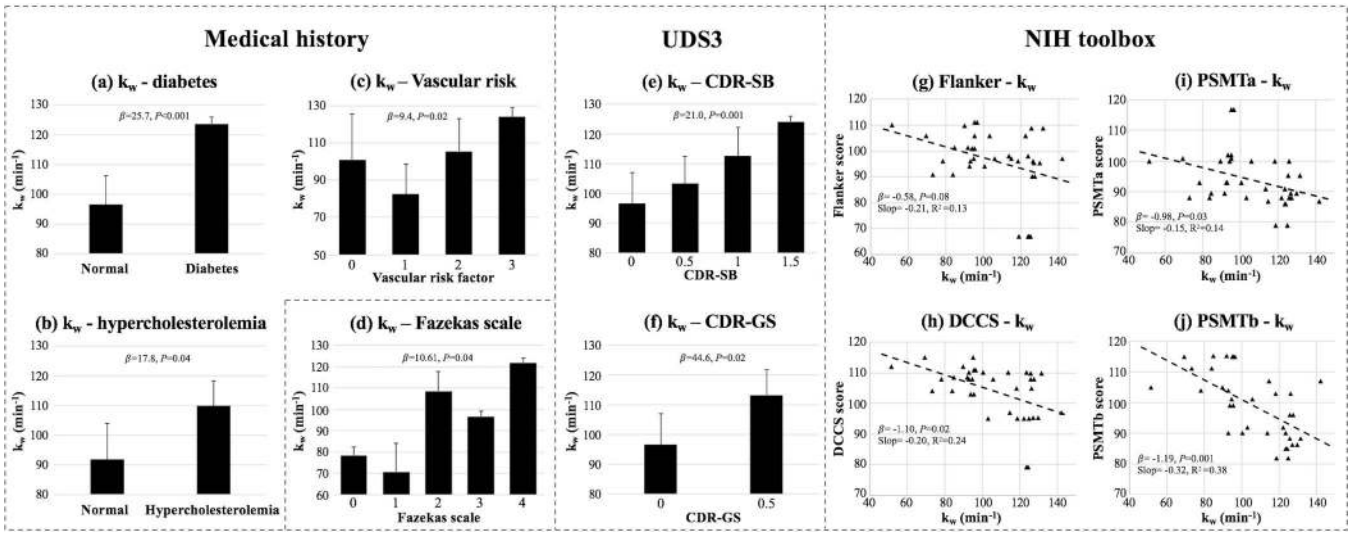

Figure 7.

(a-b): Bar plot of average k_w in normal subjects versus subjects with diabetes (a) and hypercholesterolemia (b). (c) Bar plot of average k_w versus vascular risk factors. (d) Bar plot of average kw versus Fazekas scale. (e-f): Bar plot of average k_w versus clinical dementia rating scales CDR-SB (e) and CDR-GS (f). (g-j): Scatter plots of average k_w versus NIH toolbox measurements: Flanker (g), DCCS (h), PSMTa (i) and PSMTb (j). Error bars in bar plot indicate standard deviation of k_w across subjects. Mixed effects regression coefficients β and P values are listed in bar/scatter plots. Slopes and R^2 of linear regressions (without controlling age/gender, indicated by the black dashed lines) are listed in each scatter plot.

Table 1.

Summary of clinical assessments performed in this study.

Measurement			Statistics/Description	
Medical history	Hypertension		13 subjects (68.4%)	
	Diabetes		6 subjects (31.6%)	
	Hypercholesterolemia		14 subjects (73.7%)	
	Vascular risk factor		Combination of presences of hypertension, diabetes or hypercholesterolemia (rated from 0 to 3). 3/3/9/4 subjects were rated as 0/1/2/3.	
Alzheimer's Disease Centers' Uniform Data Set v3 (UDS3)	Clinical Dementia Rating scale	Sum of Boxes (CDR-SB)	Normal (0)	10 subjects (52.6%)
			Questionable cognitive impairment (≥0.5, greater scores indicate more severe impairment)	9 subjects (47.4%)
		Global score (CDR-GS)	Normal (0)	10 subjects (52.6%)
			Questionable cognitive impairment (0.5)	9 subjects (47.4%)
	Montreal Cognitive Assessment (MoCA)		A measure of visuospatial construction, executive function, verbal memory, attention, working memory, language and orientation; Score ≥26 considered as normal (score range 0–30).	
NIH toolbox	Flanker		The Flanker is a measure of attention and inhibitory control; *Higher* Flanker scores indicate *higher* level of ability to attend to relevant stimuli and inhibit attention from irrelevant stimuli.	
	Dimensional Change Card Sort Test (DCCS)		The DCCS is a measure of cognitive flexibility; *Higher* DCCS scores indicate *higher* level of cognitive flexibility.	
	Picture Sequence Memory Test (PSMT, version a and b)		The PSMT is a measure of episodic memory, which involves the acquisition, storage and effortful recall of new information; *Higher* PSMT scores indicate *better* episodic memory.	
	Pattern Comparison Processing Speed Test (PCPS)		The PCPS is a measure of speed of processing for pattern comparison; *Higher* PCPS scores indicate *faster* speed of processing.	
	Pegboard Dexterity Test (dominant hand)		The test records the time (seconds) required for a participant to place and remove nine plastic pegs into a plastic pegboard; *Faster* completion time indicates *better* manual dexterity.	
	Grip Strength Test (dominant hand)		The test records the force (pounds) of a participant squeezing a digital hand dynamometer; *Greater* force indicates *greater* strength.	
	4-meter Walking Gait Speed Test		The test records the time (seconds) required for a participant to walk 4 meters at usual pace; *Shorter* time indicates *better* gait speed, as a measure of bipedal motion.	
White matter hyper-intensity (WMH)	Volume		Volume of WMH regions manually measured by clinical fellows from 3D T2 FLAIR images.	
	Total Fazekas scale		Quantification of WMH lesions. Total Fazekas scale is the sum of two scales rated from 0 (absent) to 3 (large confluent areas) in periventricular white matter and deep white matter. 1/1/15/1/1 subjects were rated as 0/1/2/3/4.	

Table 2.

Average k_w and ICC values of test and retest measurements in eight ROIs related to AD.

	Average k_w (min^{-1})	ICC
Frontal	98.3±20.8	0.72
Temporal	97.8±17.3	0.54
Parietal	100.6±22.2	0.52
Hippocampus	101.7±22.4	0.30
Para hippocampal gyrus	88.9±21.8	0.17
Anterior cingulum	106.6±21.9	0.74
Posterior cingulum	108.6±22.5	0.57
Precuneus	102.4±19.9	0.63

Table 3.

Repeated measures mixed effects linear regression coefficients β. P values are listed in the parentheses. Significant correlations with P values smaller than 0.05 and 0.005 are indicated by asterisks in the table.

		Clinical						UDS		
		Age	Gender (F-0, M-1)	Hyper-tension	Diabetes	Hypercho-lesterolemia	Vascular risk	CDR-SB	CDR-GS	MoCA
k_w	Whole brain	0.49 (0.43)	−10.3 (0.28)	−2.6 (0.78)	25.7** (<0.001)	17.8* (0.04)	9.4* (0.02)	21.0** (0.001)	44.6** (0.002)	−0.86 (0.45)
	GM	0.46 (0.43)	−9.2 (0.31)	−2.8 (0.75)	24.5** (<0.001)	16.7* (0.05)	8.8* (0.02)	20.3** (0.001)	43.7** (0.002)	−0.79 (0.46)
	WM	0.44 (0.50)	−11.5 (0.26)	−1.8 (0.85)	26.2** (0.001)	20.2* (0.03)	10.3* (0.01)	22.2** (0.001)	46.9** (0.003)	−0.95 (0.41)

		NIH toolbox								WMH	
		Flanker	DCCS	PSMTa	PSMTb	PCPS	Dexterity	Strength	WGS	Volumes	Fazekas scale
k_w	Whole brain	−0.58 (0.08)	−1.10* (0.02)	−0.98* (0.03)	−1.19** (0.001)	−0.37 (0.28)	1.59 (0.15)	0.24 (0.68)	2.29 (0.70)	1.68 (0.20)	10.61* (0.04)
	GM	−0.57 (0.07)	−1.09* (0.01)	−0.97* (0.02)	−1.15** (<0.001)	−0.35 (0.28)	1.51 (0.15)	0.24 (0.67)	2.33 (0.68)	1.72 (0.16)	10.53* (0.03)
	WM	−0.57 (0.12)	−1.09* (0.03)	−0.99* (0.04)	−1.31** (<0.001)	−0.37 (0.31)	1.52 (0.20)	0.30 (0.63)	2.70 (0.68)	1.75 (0.21)	11.07* (0.04)